Journal of Microbiology, Immunology and Infection 59 (2026) 107–116

Contents lists available at ScienceDirect

Journal of Microbiology, Immunology and Infection

journal homepage: www.e-jmii.com

NADPH Oxidase 4 Deficiency Enhances Dendritic Cell-mediated IL-12 Production and Th1 Responses in *Mycobacterium tuberculosis* Infection

Seunghyun Lee [a,c], Hongmin Kim [a,c], Yura Ha [a], Hong-Hee Choi [a], Lee-Han Kim [a], Sangwon Choi [a], Kyungmin Kim [a], Ji-Hwan Ryu [b], Sung Jae Shin [a,*,d], Ju Mi Lee [a,**,d]

[a] *Department of Microbiology, Institute for Immunology and Immunological Disease, Graduate School of Medical science,Brain Korea 21 Project, Yonsei University College of Medicine, Seoul, South Korea*

[b] *Department of Biomedical Sciences, Graduate School of Medical Science, Brain Korea 21 Project, Yonsei University College of Medicine, Seoul, South Korea*

ARTICLE INFO

Keywords:
Dendritic cells
Interleukin-12p70
Mycobacterium tuberculosis
NADPH oxidase 4
Type 1 T helper cells

ABSTRACT

Background: Mycobacterium tuberculosis (Mtb) infection triggers oxidative stress, necessitating host mechanisms to maintain redox balance. The NADPH oxidase (NOX) family, which produces reactive oxygen species, plays an integral part in this process. While the protective role of NOX2 in Mtb infection is well-studied, the function of NOX4 remains unclear.

Methods: To investigate the impact of NOX4, we infected C57BL/6 wild-type (WT) and NOX4-deficient (*Nox4*$^{-/-}$) mice with the Mtb K strain, assessing bacterial burdens, lung pathology, and immune responses. Then, we analyzed cytokine production and signaling pathways to explore the interaction between dendritic cells (DCs) and T cells.

Results: Nox4$^{-/-}$ mice exhibited reduced bacterial burden and milder lung pathology compared to WT mice, accompanied by increased DC infiltration and a higher frequency of CD4^{+} T cells of the Th1 subset that secrete interferon-gamma (IFN-γ) in the lungs. Interestingly, *ex vivo* experiments showed no significant difference in IFN-γ production by T cells from WT and *Nox4*$^{-/-}$ mice when activated using antibody-coated beads. However, Mtb-infected bone marrow-derived DCs (BMDCs) from *Nox4*$^{-/-}$ mice markedly enhanced IFN-γ production in WT T cells. Further investigation into the role of NOX4 in DCs revealed that BMDCs from *Nox4*$^{-/-}$ mice infected with Mtb produced significantly higher levels of IL-12. This elevation was attributed to enhanced activation of IRF1, mediated by the AKT/GSK-3β signaling pathway.

Conclusion: NOX4 negatively regulates IL-12 production in Mtb-infected DCs, suppressing Th1-mediated immunity. Its absence enhances Th1 responses, improves immune control of Mtb. Targeting NOX4 may improve tuberculosis outcomes by strengthening host immunity.

1. Introduction

Tuberculosis (TB), caused by *Mycobacterium tuberculosis* (Mtb), remains one of the leading causes of global mortality.[1] Despite the Bacillus Calmette-Guérin (BCG) vaccine and over 20 *anti*-TB drugs, the TB burden remains high, with 10.8 million new cases reported in 2023, and a disrupted decline due to the COVID-19 pandemic.[1,2]

Reactive oxygen species (ROS) are crucial for the host defense against Mtb complex infections, with nicotinamide adenine dinucleotide phosphate oxidase (NOX) serving as a primary contributor to their generation.[3,4] Among the NOX isoforms, NOX4 plays a key role in immune regulation and fibrosis, including during infections caused by *Toxoplasma gondii*, *Listeria monocytogenes*, *Chlamydia trachomatis*, Influenza A virus, and *Staphylococcus aureus*.[5–9] It also contributes to

* Corresponding author.Department of Microbiology, Institute for Immunology and Immunological Disease, Graduate School of Medical science, Brain Korea 21 Project, Yonsei University College of Medicine, 50-1 Yonsei-ro, Seodaemun-gu, Seoul 03722, South Korea

** Corresponding author.Department of Microbiology, Institute for Immunology and Immunological Disease, Graduate School of Medical science, Brain Korea 21 Project, Yonsei University College of Medicine, 50-1 Yonsei-ro, Seodaemun-gu, Seoul 03722, South Korea

E-mail addresses: sjshin@yuhs.ac (S.J. Shin), jmlee@yuhs.ac (J.M. Lee).

[c] These authors have contributed equally to this work and share the first authorship.

[d] These authors have contributed equally to this work and share the Correspondence.

https://doi.org/10.1016/j.jmii.2025.08.004

Received 30 January 2025; Received in revised form 26 June 2025; Accepted 4 August 2025

Available online 10 August 2025

pulmonary fibrosis, such as in idiopathic pulmonary fibrosis.[10] In Mtb infection, NOX4 is linked to TB fibrosis in mesothelial cells exposed to heat-killed Mtb.[11–13]

Innate immune cells such as macrophages and dendritic cells (DCs) serve as the first line of defense against Mtb and are essential for shaping the adaptive immune responses.[14] DCs, in particular, serve as essential antigen-presenting cells linking innate and adaptive immunity by recognizing Mtb through pattern recognition receptors.[15] This triggers cytokine secretion, including interleukin-12 (IL-12), tumor necrosis factor-α (TNF-α), and IL-10, and upregulation of surface molecules (MHC-I, MHC-II, CD 40, CD80, and CD86), enabling DC migration to lymph nodes to activate T cells, producing interferon (IFN)-γ, TNF-α and IL-17.[16–18] IL-12, a key driver of the Th1 response and a heterodimer of IL-12p35 and IL-12p40, promotes Mtb protection by enhancing the survival and function of memory $CD4^+$ T cells.[19–21]

While NOX4's role in macrophage function, including polarization and proinflammatory cytokine production, is well-documented,[22,23] its impact on DCs, key orchestrators of T cell immunity, remains underexplored in the context of TB. Given the central role of DCs in shaping adaptive immunity, we hypothesized that NOX4 modulates DC function and downstream T cell responses during Mtb infection.

The current study reveals that NOX4 absence enhances DC infiltration and activation, increasing IL-12 secretion via the AKT-GSK3β-IRF1 axis. This promotes Th1 differentiation, reduces bacterial load, and mitigates inflammation, highlighting NOX4 as a potential target for boosting DC-mediated immunity in TB treatment.

2. Materials and methods

2.1. Ethics statement

All animal procedures were conducted in accordance with the guidelines set by the Korean Food and Drug Administration and received approval from the Institutional Animal Care and Use Committee at Yonsei University College of Medicine (Approval number: 2016–0178, 2019–0174, Approval date: 2016-07-04, 2020-12-31). The experiments also followed the ARRIVE 2.0 guidelines (https://arriveguidelines.org/arrive-guidelines), ensuring compliance with the essential 10 and recommended details.

2.2. Mice

Male C57BL/6N wild-type (WT) mice, aged 6–7 weeks, were obtained from Japan SLC, Inc. in Shizuoka, Japan, while age-matched *Nox4*$^{-/-}$ mice were generously provided by Dr. Ji-Hwan Ryu at Yonsei University and Dr. Yun Soo Bae at Ewha Womans University in Seoul, South Korea. Briefly, *Nox4*$^{-/-}$ mice were originally generated via homologous recombination using a targeting construct based on genomic DNA from 129/SvJ embryonic stem cells. The resulting chimeras were subsequently backcrossed onto the C57BL/6N background, as previously described.[24,25] The mice were maintained under biosafety level-3 conditions with a regulated temperature of 24 ± 1 °C, 50 ± 5 % humidity, and a 12-h light and dark phases, with unrestricted supply of food and water. After a one-week acclimatization, all mice were healthy and monitored daily until the endpoint of the infection challenge.

2.3. Preparation of Mtb K strain

The Mtb K strain (Beijing lineage) was obtained from the Korean Institute of Tuberculosis in Osong, South Korea.[26] The Mtb K strain was cultured as previously described.[26,27]

2.4. Bacterial load and lung inflammation post-Mtb infection

WT and *Nox4*$^{-/-}$ mice (n = 3–5/naive group, n = 4/infection group) were infected with the Mtb K strain via aerosol using a Glas-Col aerosol device (Terre Haute, IN, USA). The infection was calibrated to deliver an initial dose of approximately 160 colony-forming units (CFUs) per mouse, as described in previous studies.[3,28,29] At two- and four-weeks post-infection, mice were euthanized for bacterial load and lung pathology analysis. Left lung lobes were homogenized, serially diluted, and cultured on 7H10 agar supplemented with 10 % OADC and 0.5 % amphotericin B (Sigma-Aldrich). Plates were incubated (37 °C, 5 % CO_2) for 3–4 weeks to enumerate CFUs. Right superior lung lobes were fixed, paraffin-embedded, and sectioned (4–5 μm), and stained with hematoxylin and eosin (H&E) for inflammation assessment. Inflamed areas were measured using ImageJ (NIH, Bethesda, MD, USA) and expressed in mm^2.

2.5. Lung cell preparation

Lung tissues were minced and incubated in Roswell Park Memorial Institute 1640 Medium (RPMI 1640; Biowest, Nuaillé, France), supplemented with 10 % fetal bovine serum (FBS; Biowest), 0.1 % collagenase type II (Worthington-Biochem, Lakewood, NJ, USA), 1 mM $CaCl_2$, and 1 mM $MgCl_2$ at 37 °C for 30 min. After erythrocyte lysis using ACK buffer (ThermoFisher Scientific, Waltham, MA, USA), the single cells were collected.

2.6. Immune profiling by flow cytometry in Mtb-infected mice

Lung cells (4×10^5 cells/well) were seeded, blocked with anti-CD16/32 antibody, and stained with LIVE/DEAD™ and surface marker antibodies (anti-CD45, *anti*-F4/80, anti-CD11b, anti-CD11c, anti-CD90.2, *anti*-MHC-II). For intracellular cytokine analysis, the cells were stimulated with either 5 μg/ml purified protein derivative (PPD) or 1 μg/ml early secreted antigenic target 6-kDa (ESAT-6) and GolgiPlug/GolgiStop (BD Bioscience, San Jose, CA, USA) for 12 h, and stained with surface markers (anti-CD90.2, anti-CD4, anti-CD8, and anti-CD44), and intracellular *anti*-IFN-γ and *anti*-TNF-α. After washing and fixation with IC Fixation buffer (Invitrogen, Waltham, Ma, USA), cells were analyzed using a CytoFLEX S Flow Cytometer (Beckman-Coulter, IN, CA, USA) and FlowJo™ software (Tree Star, Inc., Ashland, Oregon, USA). Supplementary Table 1 contains detailed information on the antibodies.

2.7. Quantification of cytokines in Mtb-infected mice

After stimulating lung cells (4×10^5 cells/well) with either 5 μg/ml PPD or 1 μg/ml ESAT-6 for 12 h, cytokine levels (IFN-γ, TNF-α, IL-10) were quantified using ELISA kits (Invitrogen and BioLegend, San Diego, CA, USA), in accordance with the manufacturer's procedures. Supplementary Table 2 contains detailed information on the antibodies.

2.8. Generation of BMDCs and Mtb infection

BMDCs were differentiated in RPMI 1640 containing 10 % FBS, 1 % penicillin/streptomycin (P/S; Sigma-Aldrich), 50 μM β-mercaptoethanol (ThermoFisher Scientific), 0.1 mM non-essential amino acids (Sigma-Aldrich), 20 ng/ml recombinant mouse GM-CSF, and 5 ng/ml IL-4 (JW CreaGene Inc., Seongnam, South Korea) for 9 days, as outlined in previous protocols.[30–32] DC purity (>80 %) was assessed using flow cytometry with LIVE/DEAD™, anti-CD11c, and *anti*-MHC-II antibodies. Antibody details are provided in Supplementary Table 1. Following Mtb infection, supernatants were obtained, and the levels of cytokines (IL-12p70, TNF-α, IL-10) were analyzed using ELISA, as described above.

2.9. In vitro T cell proliferation and polarization by BMDC co-culture

Splenocytes from Mtb-infected WT and *Nox4*$^{-/-}$ mice were used to isolated $CD4^+$ T cells via magnetic-activated cell sorting (MACS, Miltenyi Biotec, Bergisch Gladbach, Germany) system, in accordance with

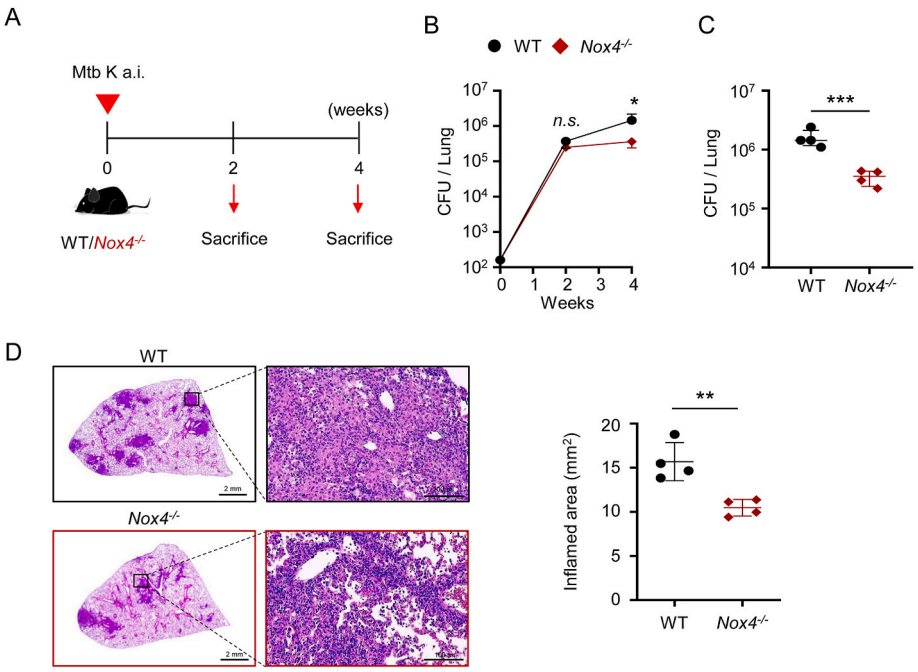

Fig. 1. Controlled bacterial burden and improved pathology in the lungs of *Nox4*$^{-/-}$ mice with Mtb infection. (A) Scheme of *in vivo* Mtb infection experiment. Mice (WT and *Nox4*$^{-/-}$) were infected with Mtb K and analyzed at two and four weeks after infection. (B) Bacterial burden in the lungs was assessed by enumerating CFUs at two- and four-weeks post-infection and presented as the kinetics. (C) The bacterial CFUs in the lungs of Mtb-infected mice were analyzed by calculating the number of colonies at four weeks post-infection and presented as scatter dot plots. (D) Inflamed areas of the lungs were analyzed by H&E staining, and inflammation in the lungs of Mtb-infected mice were quantified at four weeks post-infection (10x: scale bar = 2.0 mm; 200x: scale bar = 100 μm) and presented as scatter dot plots. This result is representative of three independent experiments. Data are shown as means ± S.D. (n = 4 mice/group). Statistical analysis was conducted by unpaired *t-test*. $^{**}p < .01$ and $^{****}p < .0001$.

Abbreviation: WT, C57BL/6N wild-type mice; *Nox4*$^{-/-}$, NOX4-deficient mice; Mtb, *Mycobacterium tuberculosis*; CFUs, Colony forming units.

the manufacturer's procedures. Cells (2×10^5 cells/well) were labeled with 1 μm of CellTrace™ violet (ThermoFisher Sientific) and co-cultured with Mtb-infected BMDCs (Multiplicity of infection [MOI] of 1, 4×10^4 cells/well) at a ratio of 1:5 between DCs and T cells for 3 days. T cell polarization was assessed by staining with fluorescent antibodies (Supplementary Table 1) and characterized through flow cytometry and FlowJo software. Supernatants were collected for IFN-γ measurement via ELISA.

2.10. RNA extraction and quantitative PCR

RNA extraction was performed utilizing TRIzol reagent (Thermo Fisher) with chloroform and isopropanol, then washed with 75 % ethanol. The RNA was eluted in DEPC-treated water and quantified using a Thermo Scientific™ NanoDrop™ 2000 Spectrophotometer. Next, cDNA was synthesized from 1 μg of RNA using an RNA-to-cDNA EcoDry™ Premix (Oligo dT) (Takara Bio, Shiga, Japan), following the manufacturer's instructions. Gene expression was quantified through quantitative PCR (qPCR) using a StepOne Real-Time PCR system (Applied Biosystems, Thermo Fisher), with *β-actin* as the housekeeping gene, and relative expression was computed using the $2^{-\Delta\Delta}$Ct method. The qPCR cycling conditions consisted of an initial 30-s denaturation at 95 °C, followed by 45 cycles of 5 s at 95 °C and 30 s at 62 °C. Supplementary Table 3 provides information on primer sequences. The data are from three independent experiments.

2.10.1. IL-12 neutralization in BMDCs and BMDC-T cell co-culture assays

WT and *Nox4*$^{-/-}$ BMDCs (1×10^6 cells/ml) were plated and subsequently infected with Mtb K at a MOI of 1. To neutralize the biological effects of IL-12, 25 μg/ml of anti-mouse IL-12 antibody (Bio X cell, Lebanon, NH, USA) was added 24 h post-infection. The cells were incubated for 1 h at 37 °C before initiating co-culture. Splenic CD4$^+$ T cells (1×10^5 cells/well), isolated from Mtb-infected WT mice using the MACS system, were co-cultured with IL-12-neutralized, Mtb-infected BMDCs (2×10^4 cells/well) at a DC to T cell ratio of 1:5 for 3 days. Following co-culture, supernatants were collected, and the levels of cytokines (IL-12p70 and IFN-γ) were quantified by ELISA, as described above.

2.11. Immunoblot analysis

BMDCs were harvested post-infection and lysed in RIPA buffer (Merck Millipore, Burlington, MA, USA) with protease and phosphate inhibitors. The supernatants were obtained, and equal protein concentrations were loaded onto sodium dodecyl sulfate-polyacrylamide gels and then transferred to PVDF membranes (Merk Millipore). Following blocking, the membranes were exposed to primary antibodies, and subsequently incubated with HRP-conjugated secondary antibodies. The antibodies used included *anti*-IRF1, *anti*-phospho-AKT1, *anti*-AKT1, *anti*-phospho-GSK3β, *anti*-GSK3β, and β-actin. Bands were detected and analyzed with ImageJ software. Supplementary Table 4 contains detailed information on the antibodies.

2.12. Compound

SB216763, a GSK3β inhibitor (Sigma-Aldrich, Cat#S3442), was used to pretreat BMDCs at concentrations of 0.1 and 10 μM for 2 h before Mtb infection.

2.13. Statistical analysis

An unpaired *t-test* was used to assess statistical significance (GraphPad Prism version 9.00, La Jolla, CA, USA, www.graphpad.com). Data are presented as mean values with standard deviation (S.D.).

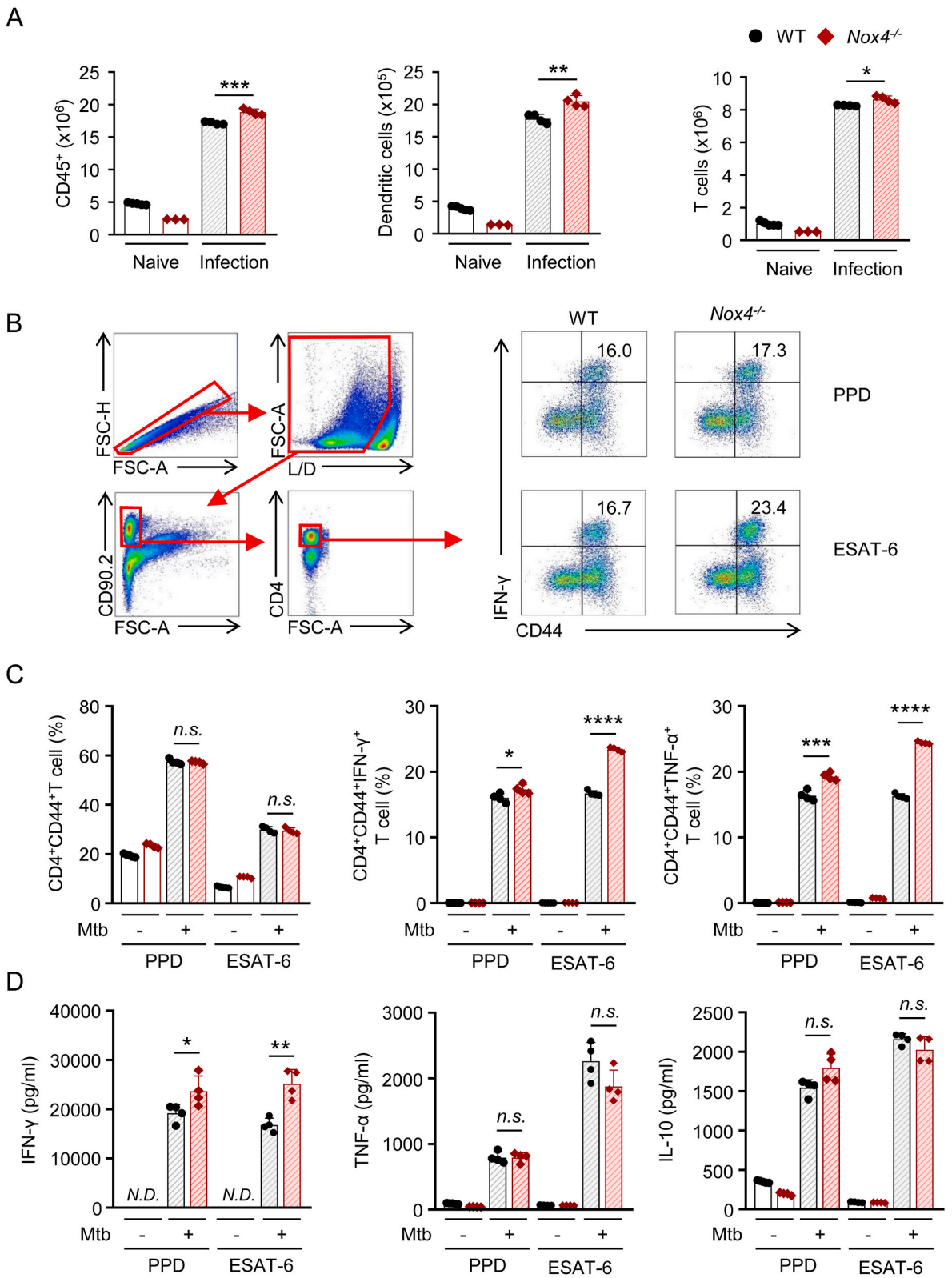

Fig. 2. Increased Mtb-specific CD4$^+$ T cell responses in *Nox4*$^{-/-}$ mice. (A) The number of infiltrated immune cells (CD45$^+$), DC (CD45$^+$CD90.2$^-$F4/80$^-$CD11b$^-$CD11c$^+$MHCII$^+$) and T cells (CD45$^+$CD90.2$^+$) in the lungs at four weeks post-infection were analyzed by flow cytometry and displayed as bar graph with dot plots. (B) Flow cytometry gating strategy was used to identify IFN-γ$^+$CD4$^+$CD44$^+$ T cells in the lungs at four weeks post-infection. The pseudocolor dot plot shows the frequency of IFN-γ$^+$CD4$^+$CD44$^+$ T cells after *ex vivo* stimulation with 5 μg/ml PPD and 1 μg/ml ESAT-6 in the lungs at four weeks post-infection. (C) The proportions of IFN-γ$^+$CD44$^+$CD4$^+$ T cells and TNF-α$^+$CD44$^+$CD4$^+$ T cells were analyzed by flow cytometry and illustrated as the bar graphs with dot plots. (D) Secreted levels of IFN-γ, TNF-α and IL-10 in suspended lung single cells after *ex vivo* stimulation with 5 μg/ml PPD and 1 μg/ml ESAT-6 were determined by ELISA and represented as bar graph accompanied by dot plots. This result is representative of three independent experiments. Data are shown as means ± S.D. (n = 3–5 mice/naive group, n = 4 mice/infection group). Statistical analysis was conducted by unpaired *t-test*. *$p < .05$, **$p < .01$, ***$p < .001$, and *n.s.*: not significant. Abbreviation: PPD, Purified protein derivative; ESAT-6, Early secreted antigenic target 6-kDa; *N.D.*, Not detected.

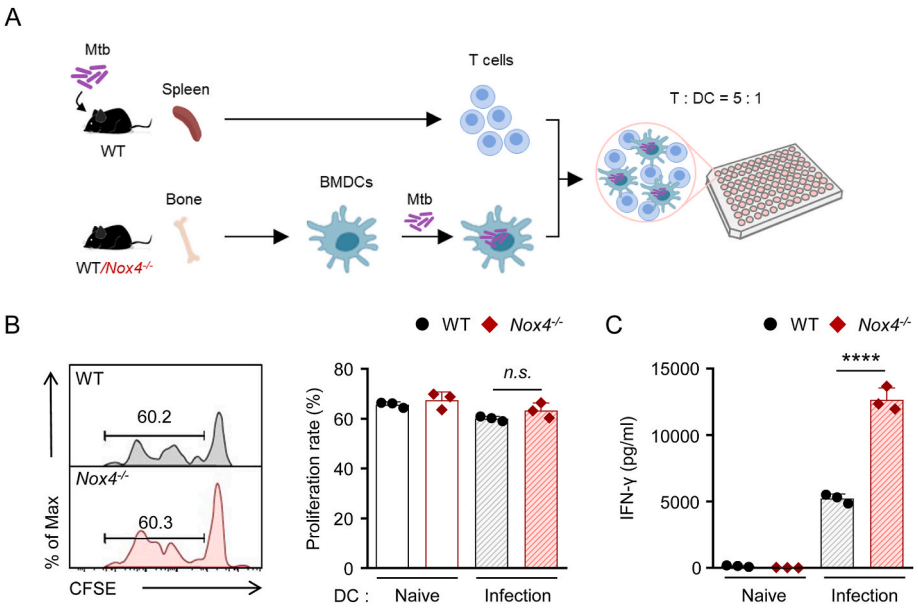

Fig. 3. Enhanced IFN-γ production in T cells by co-culturing with *Nox4*$^{-/-}$ BMDCs.
(A) Scheme of DC-T cell co-culture. Splenic CD4$^+$ T cells, isolated from Mtb infected WT mice, and BMDCs from mice (WT and *Nox4*$^{-/-}$) were infected with Mtb K for 24 h and then co-cultured for three days. (B) Proliferation rate in BMDC-WT CD4$^+$ T cell co-culture were assessed using flow cytometry. The representative proliferation rate was shown by histogram and presented as bar graphs with dot plots. (C) IFN-γ production levels in BMDC-WT CD4$^+$ T cell co-culture supernatant was determined by ELISA and shown in bar graphs with dot plots. The experiments were independently repeated at least three times, and the results from a representative experiment are presented. Data are shown as means ± S.D. Statistical analysis was conducted by unpaired *t-test*. ****$p < .0001$, and *n.s.*: not significant.
Abbreviation: BMDCs, Bone marrow-derived dendritic cells.

Significance levels were marked as *$p < .05$, **$p < .01$, ***$p < .001$ and ****$p < .0001$.

3. Results

3.1. NOX4 deficiency alleviated the bacterial burden and lung pathology in Mtb-infected mice

To explore the involvement of NOX4 in the development of TB, we utilized an infection model involving WT and *Nox4*$^{-/-}$ mice aerosol-infected with Mtb (Fig. 1A). Mice were sacrificed at two and four weeks after infection to evaluate CFUs and histopathological changes. Between two- and four-weeks post-infection, Mtb exhibited significant growth in WT mice, whereas no detectable growth was observed in *Nox4*$^{-/-}$ mice (Fig. 1B). Consistently, at four weeks post-infection, *Nox4*$^{-/-}$ mice demonstrated a notable reduction in bacterial load relative to WT mice (Fig. 1C). Histopathological analysis further confirmed a reduction in pulmonary inflammation in Mtb-infected *Nox4*$^{-/-}$ mice, consistent with the observed differences in bacterial load (Fig. 1D). Additionally, a comparable pattern was observed in the female mice group and BCG-vaccinated group (Fig. S1). These results indicate that the absence of NOX4 could contribute to regulating mycobacterial proliferation and lung inflammation.

3.2. NOX4 deficiency increased Th1 response in the lungs in Mtb-infected mice

Given that immune activation typically triggers a pro-inflammatory response in the lungs 2–3 weeks post-infection,[33,34] and that differences in bacterial burdens appear at 4 weeks in Fig. 1, we next analyzed immune cell profiles using flow cytometry at four weeks post-infection (Fig. S2A). Notably, the lungs of *Nox4*$^{-/-}$ mice exhibited a marked increase in the CD45$^+$ immune cell populations, especially DCs and T cells, following Mtb infection (Fig. 2A). However, there were no notable differences in the alveolar and interstitial macrophage counts between Mtb-infected WT and *Nox4*$^{-/-}$ mice (Fig. S2B). Based on the considerable increase in T cell populations in Mtb-infected *Nox4*$^{-/-}$ mice, we next explored whether NOX4 deficiency influences T cell responses after stimulation with 5 μg/ml PPD and 1 μg/ml ESAT-6, respectively, as outlined in the gating strategy of flow cytometry (Fig. 2B). *Ex vivo* stimulation of lung cells with PPD and ESAT-6 revealed similar percentages of CD4$^+$CD44$^+$ T cells in *Nox4*$^{-/-}$ and WT mice, but PPD and ESAT-6-specific CD4$^+$CD44$^+$ T cells producing IFN-γ$^+$ and TNF-α$^+$ were significantly more abundant in *Nox4*$^{-/-}$ mice compared to WT mice (Fig. 2C). In contrast, CD8$^+$ CD44$^+$ T cells producing IFN-γ$^+$ after PPD and ESAT-6 stimulation showed no significant differences between *Nox4*$^{-/-}$ and WT mice (Fig. S3). Furthermore, we examined cytokine production in lung cells from Mtb-infected *Nox4*$^{-/-}$ and WT mice after *ex vivo* PPD and ESAT-6 stimulation. Only IFN-γ production was significantly higher in *Nox4*$^{-/-}$ mice (Fig. 2D). Collectively, these results highlight NOX4 as an essential regulator of IFN-γ production in the immune response to Mtb infection.

3.3. NOX4 deficiency enhanced IFN-γ production in T cells interacting with Mtb-infected DCs

To investigate the role of NOX4 in Th1 immune response, we assessed CD4$^+$ T cell proliferation and IFN-γ production after anti-CD3/CD28 stimulation (Fig. S4A). T cell proliferation and IFN-γ production were similar between WT and *Nox4*$^{-/-}$ T cells, indicating that NOX4 does not affect the intrinsic function of T cells (Fig. S4B–D). In addition, exogenous IFN-γ stimulation did not significantly alter the ability of BM-derived macrophages to control Mtb growth (Fig. S4E). Then, we co-cultured splenic CD4$^+$ T cells from Mtb-infected WT mice with Mtb-infected BMDCs (5:1 ratio) for 3 days (Fig. 3A). The expression of MHC-I, MHC-II, and co-stimulatory molecules on BMDCs was comparable in both groups (Fig. S5), and T cell proliferation remained unchanged (Fig. 3B). Furthermore, NOX4 deficiency did not alter total ROS levels in BMDCs following Mtb infection (Fig. S6). However, a marked increase in IFN-γ production was observed in T cells co-cultured with *Nox4*$^{-/-}$ BMDCs, indicating enhanced T cell activation mediated by these BMDCs (Fig. 3C). These results underscore that activated *Nox4*$^{-/-}$

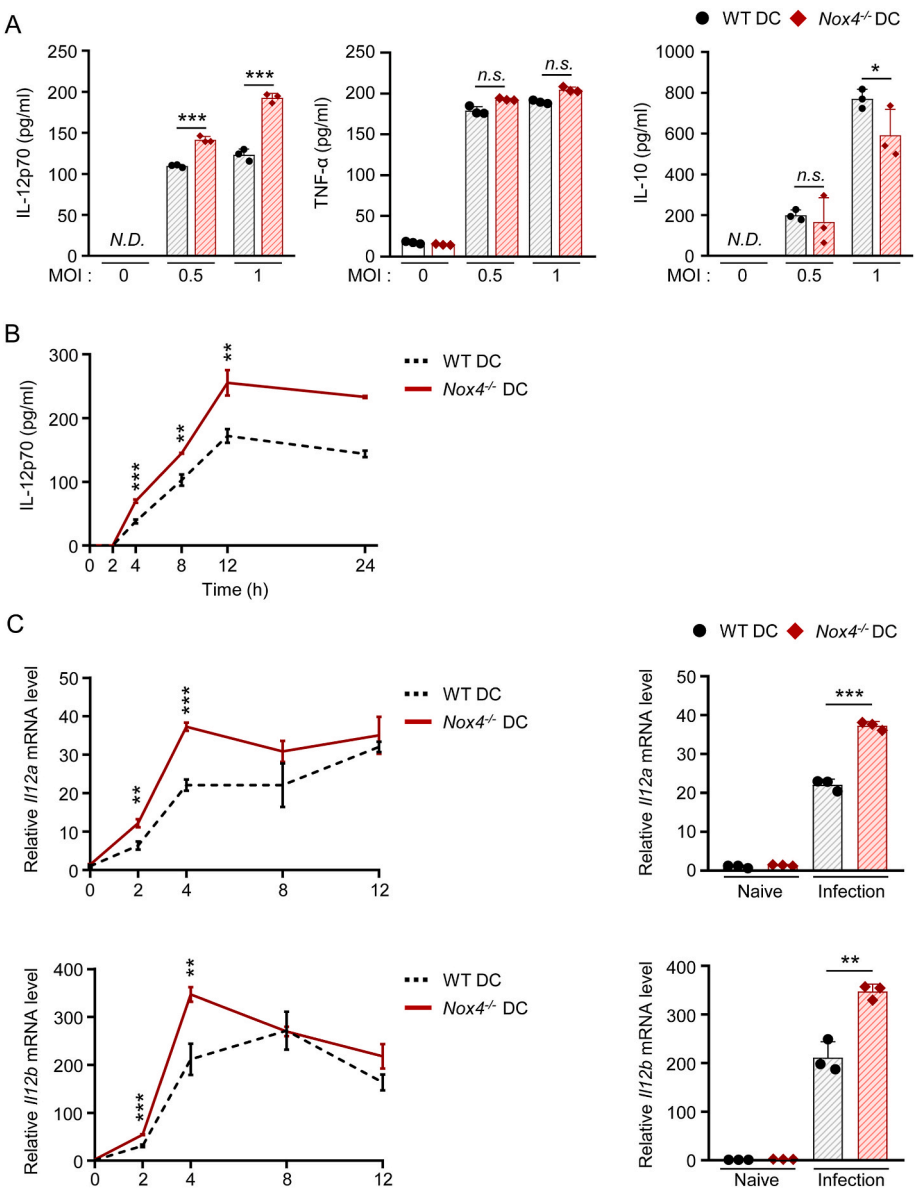

Fig. 4. Increased IL-12p70 production in Mtb-infected *Nox4*$^{-/-}$ BMDCs. (A) MOI-dependent response of cytokine production in Mtb-infected BMDCs at 24 h. Secreted IL-12p70, TNF-α and IL-10 were determined by ELISA and displayed in bar graphs with dot plots. (B) Time-dependent response of IL-12p70 in Mtb-infected BMDCs was determined by ELISA and visualized through line graphs. (C) Time-dependent mRNA expression levels of *Il12a* and *Il12b* in Mtb-infected BMDCs were measured by qPCR and are presented as bar graphs with individual data points shown for the 4 h post-infection time point. *β-actin* was used as the normalization control. The experiments were independently repeated at least three times, and the results from a representative experiment are presented. Data are shown as means ± S.D. Statistical analysis was conducted by unpaired *t-test*. *$p < .05$, **$p < .01$, ***$p < .001$ and *n.s.*: not significant.
Abbreviation: MOI, Multiplicity of infection; *N.D.*, Not detected.

BMDCs promote Th1 polarization and IFN-γ production.

3.4. NOX4 deficiency increased IL-12 production in Mtb-infected DCs

After confirming NOX4 expression in WT BMDCs and its absence in *Nox4*$^{-/-}$ BMDCs (Fig. S7), we next analyzed cytokine profiles of BMDCs from WT and *Nox4*$^{-/-}$ mice following Mtb infection. *Nox4*$^{-/-}$ BMDCs secreted higher IL-12p70 levels in an MOI-dependent manner, with no changes in TNF-α and reduced IL-10 compared to WT BMDCs (Fig. 4A). IL-12p70 levels in *Nox4*$^{-/-}$ BMDCs increased significantly at 4 h post-infection, peaking at 12 h, compared to WT BMDCs (Fig. 4B). Since IL-12p70 consists of two subunits, we examined *Il12a* (encoding IL-12p35) and *Il12b* (encoding IL-12p40) mRNA levels, which were higher in *Nox4*$^{-/-}$ BMDCs, peaking at 4 h post-infection (Fig. 4C). To determine the functional significance of IL-12p70 upregulation, neutralizing antibodies were applied during the BMDCs-T cell co-culture (Fig. 5A). Effective blockade was confirmed by a reduction in IL-12p70 levels measured by ELISA in BMDCs treated with 25 μg/ml IL-12 neutralizing antibody (Fig. 5B). Although IL-12 neutralization may not completely suppress IFN-γ secretion, it significantly reduced IFN-γ levels (Fig. 5C), thereby confirming that the elevated IL-12p70 in *Nox4*$^{-/-}$ BMDCs plays an essential role in driving Th1 activation (Fig. 5C). These findings indicate that NOX4 regulates Mtb-specific IL-12p70 expression in BMDCs, promoting Th1 activation.

3.5. NOX4 regulated IL-12 production via AKT1-GSK-3β-IRF1 axis in Mtb-infected DCs

To identify transcription factors regulating IL-12p70 secretion under NOX4 deficiency, we performed an RT^2 profiler PCR array at 4 h

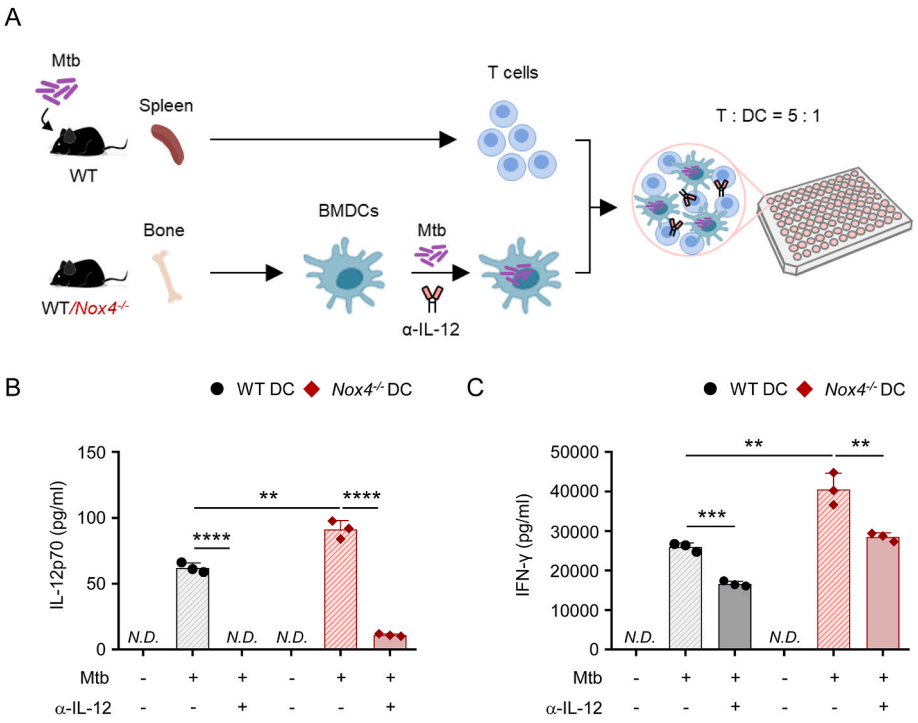

Fig. 5. Reduced IFN-γ production upon IL-12 neutralization in BMDC-T cell co-culture. (A) Scheme of BMDC-T cell co-culture with IL-12 neutralization. BMDCs from mice (WT and *Nox4*$^{-/-}$) were infected with Mtb K for 24 h, followed by treatment with anti-mouse IL-12 antibody (25 μg/ml). After 1 h of neutralization, Splenic CD4^{+} T cells isolated from Mtb infected WT mice were co-cultured with BMDCs for three days. (B) IL-12p70 levels in the supernatants of Mtb-infected BMDCs was measured by ELISA at 24 h post-infection, following IL-12 neutralization 1 h prior to infection, and are shown as bar graphs with dot plots. (C) IFN-γ level in BMDC-WT CD4^{+} T cell co-culture supernatant was determined by ELISA after 3 days and shown in bar graphs with dot plots. The experiments were independently repeated at least three times, and the results from a representative experiment are presented. Data are shown as means ± S.D. Statistical analysis was conducted by unpaired *t-test*. $^{**}p < .01$, $^{***}p < .001$ and $^{****}p < .0001$.
Abbreviation: α-IL-12, Anti-mouse IL-12 antibody; *N.D.*, Not detected.

post-infection. Among 24 differentially expressed genes in *Nox4*$^{-/-}$ BMDCs compared to WT BMDCs, 22 were upregulated and 2 were downregulated (Fig. S8A and Supplementary Table 5). The top two genes, *Nfatc4* and *Foxa2*, were validated by qPCR for the array (Fig. S8B). Using STRING, a tool for predicting protein-protein associations, we identified *Irf1* and *Jun* as direct interactors with *Il12a* and *Il12b* (Fig. S8C). Given the pivotal role of IRF1 in IL-12p70 production, we examined its activation in Mtb-infected *Nox4*$^{-/-}$ BMDCs. The mRNA expression levels of *Irf1* and *Jun* were validated. While *Irf1* was significantly upregulated in *Nox4*$^{-/-}$ BMDCs, *Jun* expression remained unchanged (Fig. S8D). Moreover, IRF1 protein expression level was significantly elevated at 4, 8, and 12 h post-infection compared to WT BMDCs (Fig. 6A and B). Since IRF1 activation is influenced by GSK-3β dephosphorylation and suppressed by AKT1 via GSK-3β phosphorylation,[35,36] we investigated AKT1 and GSK-3β regulation by NOX4. In *Nox4*$^{-/-}$ BMDCs, p-AKT1 and p-GSK-3β expression levels were significantly reduced at 30- and 60-min post-infection compared to WT BMDCs (Fig. 6C–E). To determine whether GSK-3β regulates IRF1 activation, we assessed IRF1 expression level following treatment with 0.1 or 10 μM SB216763, a selective GSK-3 inhibitor (Fig. 6F and G). Notably, 10 μM SB216763 significantly reduced IRF1 expression in Mtb-infected *Nox4*$^{-/-}$ BMDCs. Consequently, IL-12p70 secretion was also significantly decreased under the same conditions, whereas no significant effects were observed in WT BMDCs (Fig. 6H). These results demonstrate that increased IL-12p70 expression in Mtb-infected *Nox4*$^{-/-}$ BMDCs is driven by the modulation of the AKT1-GSK-3β-IRF1 signaling pathway.

4. Discussion

In the current study, we aimed to investigate the potential role of NOX4 in adaptive immune responses during Mtb infection and underlying mechanisms *in vivo* and *in vitro*. To comprehensively assess the involvement of NOX4 across sexes, *in vivo* experiments were meticulously conducted four times, encompassing both male and female mice. Strikingly, *Nox4*$^{-/-}$ mice exhibited a significant reduction in bacterial burden and lung pathology compared to WT mice, irrespective of sex. Given the higher prevalence of TB in males,[37–39] our investigation primarily focused on elucidating the role of NOX4 in male mice.

Under Mtb-infected conditions, the number of CD45^{+} leukocytes, DCs and T cells was also increased in the lung of *Nox4*$^{-/-}$ mice, accompanied by a significant elevation in IFN-γ levels, suggesting that NOX4 deficiency may influence both immune cell composition and function during Mtb infection. As previously reported that DCs act as key mediators in recognizing and presenting antigens, orchestrating T cell activation to combat TB infection.[40] Our study demonstrated that NOX4 deficiency enhances DC activation, leading to heightened CD4^{+} T cell responses. *Nox4*$^{-/-}$ BMDCs exhibited increased IL-12 production, driving elevated IFN-γ producing CD4^{+} T cells. These findings highlight the absence of NOX4 could bolster the immune responses of DCs in the context Mtb infection, suggesting a potential avenue for improved TB control.

Our study showed that *Nox4*$^{-/-}$ BMDCs enhanced the CD4^{+} T cell-derived IFN-γ production, with this effect not attributed to *Nox4*$^{-/-}$ T cells themselves. IFN-γ is a critical cytokine in the host defense against Mtb infection by activating macrophages and recruiting additional immune cells.[41,42] Previous studies have shown that Mtb uses several mechanisms to inhibit DC maturation and, specifically, suppress IL-12 secretion, thus impairing the development of protective T-cell response.[43,44] The results highlighted the role of NOX4 in regulating IL-12 and activating immune responses in DCs during Mtb infection.

In *Nox4*$^{-/-}$ BMDCs, reduced AKT1 phosphorylation was linked to increased IL-12 secretion. Previous studies reported that AKT1

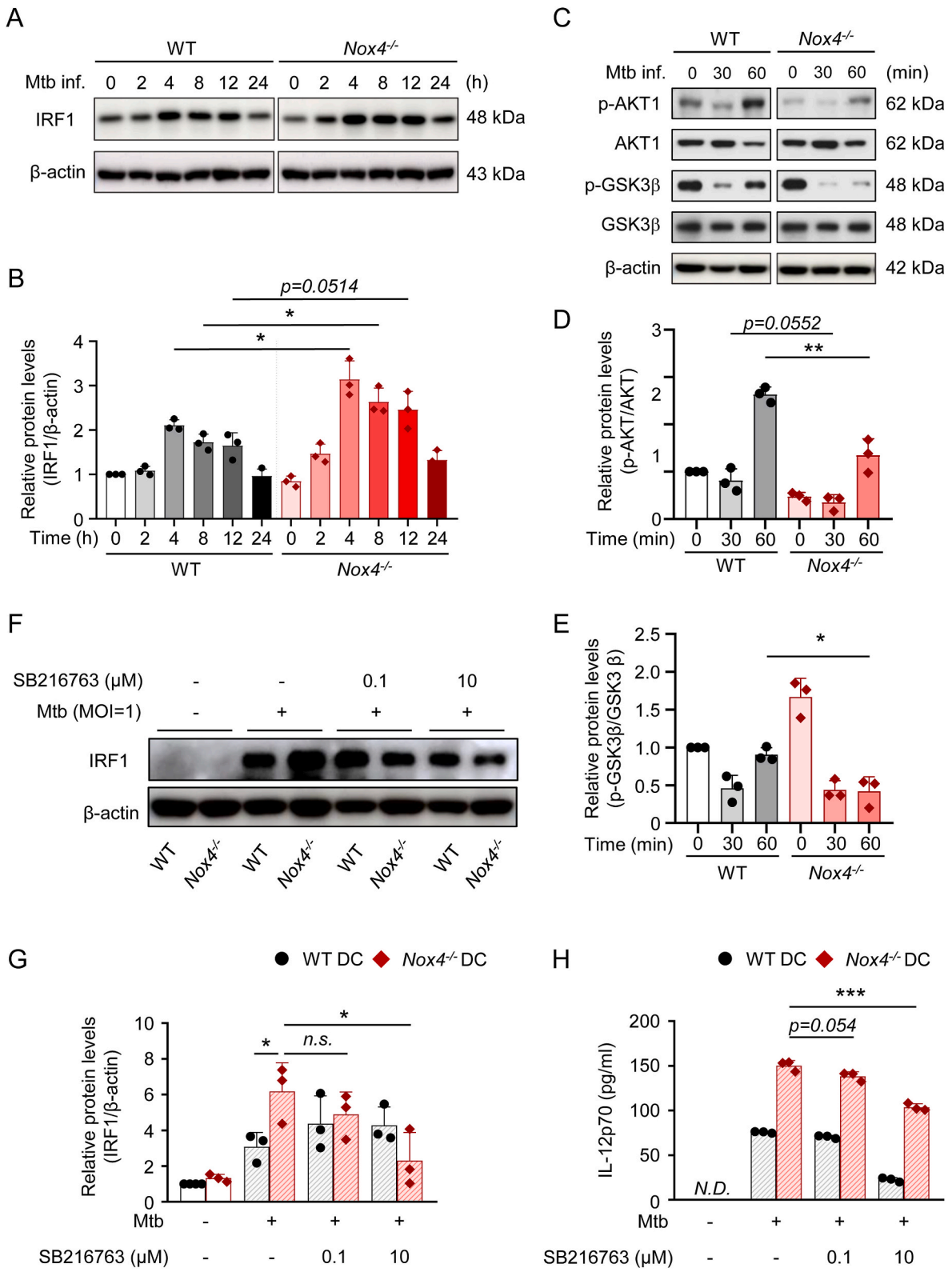

Fig. 6. IL-12 upregulation in *Nox4*$^{-/-}$ BMDCs via AKT1-GSK-3β-IRF1 axis. (A) Representative immunoblots of the expression of IRF1 and β-actin were displayed. (B) Relative fold change in protein expression of IRF1 in Mtb-infected BMDCs was shown in bar graphs with dot plots. (C) Representative immunoblots of the expression of Phosphorylated AKT1, Phosphorylated GSK-3β and β-actin were displayed. (D–E) Relative fold change in protein expression of (D) AKT1 and (E) GSK-3β in Mtb-infected BMDCs were shown in bar graphs with dot plots. (F) Representative immunoblots of IRF1 and β-actin expression at 8 h post-infection are shown, following pretreatment of BMDCs with the GSK-3β inhibitor (SB216763) 2 h prior to Mtb infection. (G) Relative fold change in protein expression of IRF1 in Mtb-infected BMDCs at 8 h post-infection is shown in bar graphs with dot plots. (H) IL-12p70 production was measured in the supernatants of Mtb-infected BMDCs after 24 h by ELISA and presented as bar graphs with dot plots. The experiments were independently repeated at least three times, and the results from a representative experiment are presented. Data are shown as means ± S.D. Statistical analysis was conducted by unpaired *t-test*. *$p < .05$, **$p < .01$, and *n.s.*: not significant. Abbreviation: Inf., Infection; *N.D.*, Not detected.

activation inhibits GSK3β activity by phosphorylating serine 9, reducing IL-12 secretion.[45,46] Conversely, GSK3β activation promotes IRF-1 degradation by phosphorylating its T181 residue, and IRF-1 is crucial for IL-12 production in DCs.[35,36] Although the detailed mechanistic hierarchy among GSK3β, IRF1, and IL-12 regulation remains incompletely defined, our data suggest that IRF1 expression is modulated in response to changes in GSK3β activity, supporting a sequential link between these factors in IL-12 production. We exhibited that *Nox4*$^{-/-}$ BMDCs showed reduced GSK3β phosphorylation and increased IRF-1 expression during Mtb infection. This suggests that lower AKT1 phosphorylation in *Nox4*$^{-/-}$ BMDCs reduces GSK3β phosphorylation, increasing IRF1 expression, and enhancing IL-12 production, which drives a protective T cell response. These findings align with the observation that *Nox4*$^{-/-}$ BMDCs are more effective at promoting CD4^{+} T cell responses and IFN-γ production.

This study has three limitations. First, given that NOX4 is known to influence the differentiation of various immune cell populations, there may be baseline differences in immune cell composition between WT and *Nox4*$^{-/-}$ mice.[47,48] We did not directly assess these differences, and we could not rule out the possibility that such variations contributed to our findings. Future studies are needed to investigate this aspect. Second, while our findings demonstrate that IL-12p70 is a key mediator of enhanced Th1 activation in *Nox4*$^{-/-}$ BMDCs, IFN-γ production remained higher in T cells co-cultured with *Nox4*$^{-/-}$ DCs compared to WT DCs even after IL-12 neutralization. One possible explanation is that the fixed concentration of neutralizing antibody may not have been sufficient to block the elevated baseline IL-12p70 in *Nox4*$^{-/-}$ DCs. Alternatively, additional IL-12-independent mechanisms, such as altered cytokine profiles or increased co-stimulatory signaling, may have contributed to the residual Th1 response. Further investigation is warranted to elucidate these pathways and fully define the immunoregulatory role of NOX4. Third, the activation of the PI3K/Akt pathway by NOX4 is consistent with previous studies conducted in various cellular contexts, such as non-small cell lung cancer and hepatic stellate cells.[23,49,50] However, these studies described this activation as ROS-dependent. In immune cells, the role of NOX4 in ROS generation remains controversial and appears to vary depending on the type of stimulus and cellular context.[22,51] For instance, Lee et al. demonstrated that NOX4 knockdown or overexpression altered ROS levels in macrophages stimulated with oxidized LDL.[51] In contrast, Helfinger et al. reported that NOX4-deficient macrophages exhibited increased ROS production following LPS and IFN-γ stimulation, which was attributed to compensatory upregulation of NOX2, along with enhanced NF-$_k$B activation and proinflammatory cytokine expression.[22] These conflicting findings highlight the complexity of NOX4-mediated signaling and suggest that NOX4's contribution to ROS production is context- and stimulus-dependent. In our study, however, we observed NOX4-dependent Akt activation without a significant difference in ROS levels between WT and *Nox4*$^{-/-}$ BMDCs, suggesting a ROS-independent mechanism in this context. The precise role of ROS in this signaling cascade remains unclear and warrants further investigation.

In summary, our study demonstrates that NOX4 deficiency enhances IL-12 production via the AKT-GSK3β-IRF1 pathway in DCs, boosting IFN-γ production in CD4^{+} T cells and aiding in Mtb control. These results emphasize the importance of NOX4 in regulating the interactions between DCs and T cells in the context of Mtb infection. Targeting NOX4 with inhibitors could promote Th1 responses, offering a potential strategy for TB control and vaccine development. Further research on NOX4 inhibitors in DCs could aid TB vaccine adjuvant development.

CRediT authorship contribution statement

Seunghyun Lee: Writing – review & editing, Writing – original draft, Visualization, Validation, Methodology, Investigation, Formal analysis. **Hongmin Kim:** Writing – review & editing, Writing – original draft, Visualization, Validation, Methodology, Investigation. **Yura Ha:** Writing – review & editing, Investigation. **Hong-Hee Choi:** Writing – review & editing, Investigation. **Lee-Han Kim:** Writing – review & editing, Validation. **Sangwon Choi:** Writing – review & editing, Validation. **Kyungmin Kim:** Writing – review & editing, Validation. **Ji-Hwan Ryu:** Writing – review & editing, Resources. **Sung Jae Shin:** Writing – review & editing, Writing – original draft, Visualization, Supervision, Methodology, Investigation, Funding acquisition, Conceptualization. **Ju Mi Lee:** Writing – review & editing, Writing – original draft, Visualization, Software, Project administration, Investigation, Funding acquisition, Conceptualization.

Data availability statement

All datasets presented in the study are included in the article/Supplementary Information.

Declaration of competing interest

The authors report there are no competing interests to declare.

Acknowledgments

This research was supported by the National Research Foundation of Korea (NRF) grant, funded by the Ministry of Science and Information and Communication Technology (MSIT), South Korea (Grant No. RS-2023-00208115); by the Basic Science Research Program through the NRF, funded by the Ministry of Education, South Korea (Grant No. RS-2023-00246091); and by the National Institute of Health (KNIH) research project, South Korea (Grant No. 2024-ER2001-01).

Appendix A. Supplementary data

Supplementary data to this article can be found online at https://doi.org/10.1016/j.jmii.2025.08.004.

References

1. World Health Organization. *Global Tuberculosis Report 2024*. Geneva: World Health Organization; 2024:1–68.
2. Young C, Walzl G, Du Plessis N. Therapeutic host-directed strategies to improve outcome in tuberculosis. *Mucosal Immunol*. 2020;13:190–204.
3. Choi E, Choi HH, Kwon KW, et al. Permissive lung neutrophils facilitate tuberculosis immunopathogenesis in male phagocyte NADPH oxidase-deficient mice. *PLoS Pathog*. 2024;20, e1012500.
4. Olive AJ, Smith CM, Kiritsy MC, Sassetti CM. The phagocyte oxidase controls tolerance to *Mycobacterium tuberculosis* infection. *J Immunol*. 2018;201:1705–1716.
5. Han S, Moon S, Chung YW, Ryu JH. NADPH Oxidase 4-mediated alveolar macrophage recruitment to lung attenuates neutrophilic inflammation in *Staphylococcus aureus* infection. *Immune Netw*. 2023;23, e42.
6. Thapa J, Yoshiiri G, Ito K, et al. *Chlamydia trachomatis* requires functional host-cell mitochondria and NADPH oxidase 4/p38MAPK signaling for growth in normoxia. *Front Cell Infect Microbiol*. 2022;12, 902492.
7. Hendricks KS, To EE, Luong R, et al. Endothelial NOX4 oxidase negatively regulates inflammation and improves morbidity during influenza A virus lung infection in mice. *Front Cell Infect Microbiol*. 2022;12, 883448.
8. Kim JH, Lee J, Bae SJ, et al. NADPH oxidase 4 is required for the generation of macrophage migration inhibitory factor and host defense against *Toxoplasma gondii* infection. *Sci Rep*. 2017;7:6361.
9. Dolowschiak T, Chassin C, Ben Mkaddem S, et al. Potentiation of epithelial innate host responses by intercellular communication. *PLoS Pathog*. 2010;6, e1001194.
10. Hecker L, Logsdon NJ, Kurundkar D, et al. Reversal of persistent fibrosis in aging by targeting Nox4-Nrf2 redox imbalance. *Sci Transl Med*. 2014;6, 231ra47.
11. Woo SJ, Kim Y, Jung H, Lee JJ, Hong JY. MicroRNA 148a suppresses tuberculous fibrosis by targeting NOX4 and POLDIP2. *Int J Mol Sci*. 2022;23.
12. Woo SJ, Kim Y, Jung H, Lee JJ, Hong JY. Tuberculous fibrosis enhances tumorigenic potential via the NOX4-autophagy axis. *Cancers (Basel)*. 2021;13.
13. Kim Y, Park SY, Jung H, Noh YS, Lee JJ, Hong JY. Inhibition of NADPH oxidase 4 (NOX4) signaling attenuates tuberculous pleural fibrosis. *J Clin Med*. 2019;8.
14. Mihret A. The role of dendritic cells in *Mycobacterium tuberculosis* infection. *Virulence*. 2012;3:654–659.
15. Hossain MM, Norazmi MN. Pattern recognition receptors and cytokines in Mycobacterium tuberculosis infection–the double-edged sword? *BioMed Res Int*. 2013;2013, 179174.
16. Domingo-Gonzalez R, Prince O, Cooper A, Khader SA. Cytokines and chemokines in *Mycobacterium tuberculosis* infection. *Microbiol Spectr*. 2016;4.

17. Mihret A, Mamo G, Tafesse M, Hailu A, Parida S. Dendritic cells activate and mature after infection with *Mycobacterium tuberculosis*. *BMC Res Notes*. 2011;4:247.
18. Bafica A, Scanga CA, Feng CG, Leifer C, Cheever A, Sher A. TLR9 regulates Th1 responses and cooperates with TLR2 in mediating optimal resistance to *Mycobacterium tuberculosis*. *J Exp Med*. 2005;202:1715–1724.
19. Lyadova IV, Panteleev AV. Th1 and Th17 cells in tuberculosis: protection, pathology, and biomarkers. *Mediators Inflamm*. 2015;2015, 854507.
20. Vignali DA, Kuchroo VK. IL-12 family cytokines: immunological playmakers. *Nat Immunol*. 2012;13:722–728.
21. Gallegos AM, van Heijst JW, Samstein M, Su X, Pamer EG, Glickman MS. A gamma interferon independent mechanism of CD4 T cell mediated control of *M. tuberculosis* infection *in vivo*. *PLoS Pathog*. 2011;7, e1002052.
22. Helfinger V, Palfi K, Weigert A, Schroder K. The NADPH oxidase Nox4 controls macrophage polarization in an NFkappaB-dependent manner. *Oxid Med Cell Longev*. 2019;2019, 3264858.
23. Zhang J, Li H, Wu Q, et al. Tumoral NOX4 recruits M2 tumor-associated macrophages via ROS/PI3K signaling-dependent various cytokine production to promote NSCLC growth. *Redox Biol*. 2019;22, 101116.
24. Lee SR, Lee HE, Yoo JY, et al. Nox4-SH3YL1 complex is involved in diabetic nephropathy. *iScience*. 2024;27, 108868.
25. Lee JH, Joo JH, Kim J, et al. Interaction of NADPH oxidase 1 with toll-like receptor 2 induces migration of smooth muscle cells. *Cardiovasc Res*. 2013;99:483–493.
26. Jeon BY, Kwak J, Hahn MY, et al. *In vivo* characteristics of Korean beijing *Mycobacterium tuberculosis* strain K1 in an aerosol challenge model and in the cornell latent tuberculosis model. *J Med Microbiol*. 2012;61:1373–1379.
27. Kwon KW, Choi HH, Han SJ, et al. Vaccine efficacy of a *Mycobacterium tuberculosis* Beijing-specific proline-glutamic acid (PE) antigen against highly virulent outbreak isolates. *FASEB J*. 2019;33:6483–6496.
28. Kim H, Song EJ, Choi E, Kwon KW, Park JH, Shin SJ. Adjunctive administration of parabiotic *Lactobacillus sakei* CVL-001 ameliorates drug-induced toxicity and pulmonary inflammation during antibiotic treatment for tuberculosis. *Int Immunopharmacol*. 2024;132, 111937.
29. Kang TG, Kwon KW, Kim K, et al. Viral coinfection promotes tuberculosis immunopathogenesis by type I IFN signaling-dependent impediment of Th1 cell pulmonary influx. *Nat Commun*. 2022;13:3155.
30. Lee JM, Park J, Reed SG, et al. Vaccination inducing durable and robust antigen-specific Th1/Th17 immune responses contributes to prophylactic protection against *Mycobacterium avium* infection but is ineffective as an adjunct to antibiotic treatment in chronic disease. *Virulence*. 2022;13:808–832.
31. Choi HG, Kwon KW, Choi S, et al. Antigen-specific IFN-gamma/IL-17-co-producing $CD4^+$ T-cells are the determinants for protective efficacy of tuberculosis subunit vaccine. *Vaccines (Basel)*. 2020;8.
32. Choi HH, Kwon KW, Han SJ, et al. PPE39 of the *Mycobacterium tuberculosis* strain Beijing/K induces Th1-cell polarization through dendritic cell maturation. *J Cell Sci*. 2019;132.
33. Kolloli A, Kumar R, Venketaraman V, Subbian S. Immunopathology of pulmonary *Mycobacterium tuberculosis* infection in a humanized mouse model. *Int J Mol Sci*. 2024;25.
34. Chackerian AA, Alt JM, Perera TV, Dascher CC, Behar SM. Dissemination of *Mycobacterium tuberculosis* is influenced by host factors and precedes the initiation of T-cell immunity. *Infect Immun*. 2002;70:4501–4509.
35. Garvin AJ, Khalaf AHA, Rettino A, et al. GSK3beta-SCFFBXW7alpha mediated phosphorylation and ubiquitination of IRF1 are required for its transcription-dependent turnover. *Nucleic Acids Res*. 2019;47:4476–4494.
36. Gautier G, Humbert M, Deauvieau F, et al. A type I interferon autocrine-paracrine loop is involved in toll-like receptor-induced interleukin-12p70 secretion by dendritic cells. *J Exp Med*. 2005;201:1435–1446.
37. Davies LRL, Wang C, Steigler P, et al. Age and sex influence antibody profiles associated with tuberculosis progression. *Nat Microbiol*. 2024;9:1513–1525.
38. Gupta M, Srikrishna G, Klein SL, Bishai WR. Genetic and hormonal mechanisms underlying sex-specific immune responses in tuberculosis. *Trends Immunol*. 2022;43:640–656.
39. Marcoa R, Ribeiro AI, Zao I, Duarte R. Tuberculosis and gender - factors influencing the risk of tuberculosis among men and women by age group. *Pulmonology*. 2018;24:199–202.
40. Zhou X, Xu H, Li Q, et al. Viperin deficiency promotes dendritic cell activation and function via NF-kappaB activation during *Mycobacterium tuberculosis* infection. *Inflamm Res*. 2023;72:27–41.
41. Orme IM, Roberts AD, Griffin JP, Abrams JS. Cytokine secretion by CD4 T lymphocytes acquired in response to *Mycobacterium tuberculosis* infection. *J Immunol*. 1993;151:518–525.
42. Shimokata K, Kishimoto H, Takagi E, Tsunekawa H. Determination of the T-cell subset producing gamma-interferon in tuberculous pleural effusion. *Microbiol Immunol*. 1986;30:353–361.
43. Su H, Peng B, Zhang Z, Liu Z, Zhang Z. The *Mycobacterium tuberculosis* glycoprotein Rv1016c protein inhibits dendritic cell maturation, and impairs Th1/Th17 responses during mycobacteria infection. *Mol Immunol*. 2019;109:58–70.
44. Cooper AM, Solache A, Khader SA. Interleukin-12 and tuberculosis: an old story revisited. *Curr Opin Immunol*. 2007;19:441–447.
45. Yoeli-Lerner M, Chin YR, Hansen CK, Toker A. Akt/protein kinase b and glycogen synthase kinase-3beta signaling pathway regulates cell migration through the NFAT1 transcription factor. *Mol Cancer Res*. 2009;7:425–432.
46. Rodionova E, Conzelmann M, Maraskovsky E, et al. GSK-3 mediates differentiation and activation of proinflammatory dendritic cells. *Blood*. 2007;109:1584–1592.
47. Kim J, Kim J, Lim HJ, Lee S, Bae YS, Kim J. Nox4-IGF2 axis promotes differentiation of embryoid body cells into derivatives of the three embryonic germ layers. *Stem Cell Rev Rep*. 2022;18:1181–1192.
48. Yoshikawa Y, Ago T, Kuroda J, et al. Nox4 promotes neural stem/precursor cell proliferation and neurogenesis in the hippocampus and restores memory function following trimethyltin-induced injury. *Neuroscience*. 2019;398:193–205.
49. Zhou M, Zhao X, Liao L, et al. Forsythiaside a regulates activation of hepatic stellate cells by inhibiting NOX4-dependent ROS. *Oxid Med Cell Longev*. 2022;2022, 9938392.
50. Zhang C, Lan T, Hou J, et al. NOX4 promotes non-small cell lung cancer cell proliferation and metastasis through positive feedback regulation of PI3K/Akt signaling. *Oncotarget*. 2014;5:4392–4405.
51. Lee CF, Qiao M, Schroder K, Zhao Q, Asmis R. Nox4 is a novel inducible source of reactive oxygen species in monocytes and macrophages and mediates oxidized low density lipoprotein-induced macrophage death. *Circ Res*. 2010;106:1489–1497.